

Studies on Membrane Surfaces of A-B-A Tri-Block Copolymers Consisting of Poly(ϵ -*N*-benzyloxycarbonyl-L-lysine) as the A Component and Polybutadiene as the B Component

Kouhei KUGO, Yoshio HATA, Toshio HAYASHI,
and Akio NAKAJIMA

*Department of Polymer Chemistry, Kyoto University,
Sakyo-ku, Kyoto 606, Japan.*

(Received December 28, 1981)

ABSTRACT: The surface characteristics of A-B-A type tri-block copolymer membranes consisting of α -helical poly(ϵ -*N*-benzyloxycarbonyl-L-lysine) as the A component and polybutadiene as the B component were investigated by X-ray photoelectron spectroscopy (XPS), replication electron micrograph, and wettability measurement. The XPS measurements showed the copolymer composition of the outermost surface to be quite different from the bulk composition. It was found by replication electron micrograph that the block copolymer surface is not even, *i.e.*, the polybutadiene domains are elevated above the polypeptide matrix. The results of contact angle measurements indicated the existence of an interfacial region between the α -helical A component and the B component at the surfaces of the block copolymer membranes.

KEY WORDS Tri-Block Copolymer / Poly(ϵ -*N*-benzyloxycarbonyl-L-lysine / Polybutadiene / X-Ray Photoelectron Spectroscopy / Replication Electron Micrograph / Wettability /

Studies on membrane surfaces, *i.e.*, polymer-air interfaces, of the A-B type and A-B-A type block copolymers have been developed by Litt,¹ Rastogi,² Owen,³ Vanzo,⁴ Brash,⁵ Clark,⁶ O'Malley,⁷ and Merrill⁸ using surface free energy, contact angle, replication electron micrograph, Fourier transform IR internal reflection spectroscopy, and X-ray photoelectron spectroscopy (XPS) techniques. XPS has been applied to analyzing polymer surfaces by Clark *et al.*^{6,9,10} over the last few years. This technique complements contact angle measurements,^{6,11} since it is very sensitive to the outermost surface of few tens of angstroms in depth owing to the dependence of the escape depth λ on kinetic energy.¹² All the block copolymers used in this study consisted of components having a random coil conformation in solution.

In a previous paper,¹³ we have described the preparation and characterization of A-B-A type tri-block copolymers LBL's consisting of poly(ϵ -*N*-benzyloxycarbonyl-L-lysine) (PBCL) as the A component and polybutadiene (PB) as the B com-

ponent. As is well known, polybutadiene chains are in a random coil conformation in ordinary solvents, whereas polypeptide chains take on an α -helical conformation in a helicogenic solvent.

In this work, we have investigated the surface properties of these unusual block copolymer membranes by the XPS technique, replication electron micrograph, and contact angle measurement.

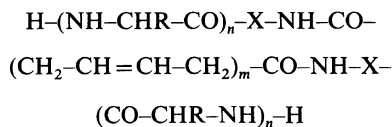
The bulk morphology of block copolymers consisting of polypeptides has been reported,¹⁴⁻¹⁶ but as yet, no study has been made on the surface properties of these copolymer membranes. Furthermore, the surface properties of copolymers having a microheterophase structure are of interest to the biomedical field in view of this possible antithrombogenicity.^{17,18}


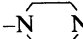
EXPERIMENTAL

Materials

The details of the preparation and characterizations of LBL tri-block copolymers are described

in the preceding paper.¹³ The LBL tri-block copolymer has the chemical structure,



where R and X denote $-(\text{CH}_2)_4-\text{NH}-\text{CO}-\text{O}-\text{CH}_2-$ , and $-\text{N}$  $-\text{CH}_2-\text{CH}_2-$, respectively. It is known that at least four peptide residues at the C-terminal of a peptide chain do not participate in the formation of α -helix.

The molecular properties of the samples used are summarized in Table I, where P_A denotes the degree of polymerization of the A block component. The casting solvent used for film preparations was a 10 : 1 (v/v) mixture of chloroform (CF) and 2,2,2-trifluoroethanol (TFE). The polymer solutions were slowly cast onto glass plates at 25°C and at a relative humidity less than 65%.

It seems to be difficult that the existence of PB component at the membrane surface of the present block copolymers is explicitly detected by XPS using the relevant component peak of the Cls levels. Hence, it is necessary to introduce some element having a high electron density into a PB component. We utilized the same technique as that for electron microscopy,¹³ *i.e.*, the reaction of osmium tetroxide (OsO_4) with olefinic double bonds existing in a PB component. The presence of a PB component was detected by the XPS peaks of the Os 4f electrons. Osmium tetroxide has long been used as a reagent for the *cis*-hydroxylation of alkenes,¹⁹ and also in electron microscopy as a staining and fixative agent

for biological tissues.^{20,21} The reaction of osmium tetroxide with olefinic C=C double bonds is usually regarded as involving stoichiometric addition, *i.e.*, one atom of Os per double bond.^{20,22} In this study, the reaction was confirmed by infrared spectra and elemental analysis before the XPS measurements.

Infrared Spectra. Qualitative Osmium Determination

Infrared (IR) spectra were measured by a Shimadzu Model-30A IR Spectrophotometer in the region of 4000 to 400 cm^{-1} . Solvent-cast films of 4 μm in thickness were stained with saturated vapor from a 4% OsO_4 aqueous solution at room temperature for 24 h. These films were dried *in vacuo* at 50°C for 24 h before use.

Elemental Analysis. Quantitative Osmium Determination

In order to check the staining with OsO_4 vapor, an elemental analysis was carried out on films 2 μm in thickness stained for 40 min, 1 h, and 24 h. The films were dried in the same manner as above before use.

XPS Sample Preparation

The LBL block copolymers and PBCL homopolymer were cast from the solvent mixture described above onto cover glass slides having the same size as the sample probe. After staining for 24 h and vacuum drying in the same manner as above, the samples were fixed on the sample probe with double-side adhesive tape.

XPS Measurements

The XPS spectra were obtained on a Shimadzu 650 B ESCA spectrometer using $\text{MgK}\alpha_{1,2}$ exciting radiation. For calibration, the Cls level emitted from the saturated hydrocarbon at 285.0 eV binding energy was employed. There was no visible damage on sample surfaces during the exposure time involved in these measurements. Argon ion etching was carried out using a Shimadzu ARE-8 Ion Etching Device. All spectra were well fitted by computer calculation, using the nonlinear least-squares technique. The line functions of individual peaks were fitted to Gaussian spectral line functions,^{23,24} and the base lines were corrected by applying the spline function. The Os 4f_{5/2}-Os 4f_{7/2} doublet obtained from each sample was computer fitted by assuming that a full width at half max-

Table I. Molecular characterization of samples prepared

Designation	$[\eta]$	Butadiene mol%	P_A	M_n $\times 10^{-4}$
	dl g^{-1} (<i>m</i> -cresol, 25°C)			
LBL-1	0.33	52.3	28	1.8
LBL-2	0.39	42.3	42	2.6
LBL-3	0.47	23.7	98	5.5
LBL-4	0.48	16.2	158	8.7
LBL-5	0.49	11.9	226	12.2
PBCL	1.83	0.0	795	41.7

imum and the splitting of each component of the doublet are common to all Os doublets. The height ratio ($4f_{5/2} : 4f_{7/2} = 0.8 : 1$) was quoted from literature data.²⁴ The best fit experimental spectra were determined empirically. The linear background was then subtracted both from the data and from the fitted curve before the net spectra were plotted.

As is well known, the intensity I of a signal is given by,

$$dI = F\alpha Nke^{-x/\lambda} dx \quad (1)$$

where F is the X-ray flux, α , the cross-section for photoionization in a given shell of a given atom for a given X-ray energy, N , the number of atoms in volume elements, k , a spectrometer factor, and λ , the electron mean-free-path. By integrating eq 1, the number ratio N_2/N_1 of atoms is obtained as,

$$\frac{N_2}{N_1} = \frac{I_2}{I_1} \times \frac{\alpha_1 \lambda_1}{\alpha_2 \lambda_2} \quad (2)$$

The PB surface compositions were estimated by using N_2/N_1 obtained from eq 2 assuming that the relative photoelectron signal intensities, $\alpha_2 \lambda_2$ and $\alpha_1 \lambda_1$, of Os 4f and Cls are 2.65 and 0.25, respectively.²⁵

Replication Electron Micrograph

To observe surface morphology of polymer membranes, a three-stage replica technique was employed with a transmission microscope. Specimens were first coated with poly(vinyl alcohol) (PVA) from an aqueous solution, and the PVA replicas were further replicated by acetylcellulose films (AC) using methyl acetate. Last of all, the AC replica was shadowed with platinum/palladium (Pt/Pd = 80 : 20) at an angle of about 30°, and backed with carbon in a vacuum evaporator. The AC was dissolved off the carbon-Pt/Pd replica in methyl acetate. The replicas were examined under a Hitachi H-500 transmission electron microscope. Moreover, in order to confirm whether the surface of polymer membranes is concave or convex, an aqueous polystyrene emulsion was sprayed over the surface of the AC replicas before shadowing with Pt/Pd.

Contact Angles

The measurement of the contact angles of various liquids on polymer surfaces was made with a Shimadzu Model ST-1 Surface Tensometer at 20°C. According to Adam's equation,²⁶ the contact angle

θ is obtained from,

$$\cos \theta = \frac{\cos \theta_a + \cos \theta_r}{2} \quad (3)$$

where θ_a and θ_r are the advancing and receding contact angles, respectively. The values of θ obtained in this study are averages of at least 5 films prepared independently.

RESULTS AND DISCUSSION

Infrared Spectra

Figure 1 shows the infrared (IR) spectra of PBCL and the LBL block copolymer films before and after 24 h reaction with OsO₄. The difference (1') between spectra before the (1) and after (1') reaction indicates that no change occurred as a result of the reaction. The same result was obtained after 1 week of reaction. The spectra of LBL-4 and LBL-1 show, in contrast, a decrease in the CH out-of-plane band modes²⁷ at 967 cm⁻¹ by the reaction. The difference spectra (2'', 3'') clearly demonstrate this fact; the decrease is found in the 967 cm⁻¹ band. These results indicate that the C=C double bonds existing in the polybutadiene component react with OsO₄.

The most remarkable difference resulting from reaction with OsO₄ is the appearance of new strong bands at 990 cm⁻¹ and 640 cm⁻¹ (2'', 3''). The former is assigned to the Os=O (terminal) stretching vibration^{22,28,29} and the latter, to the Os₂O₂ (oxygen bridge) stretching vibration characteristic of dimeric monoester complexes.²⁹ These new bands appeared more clearly in the case of LBL-1, since the butadiene content of LBL-1 was higher than that of LBL-4.

These IR spectra indicate that the osmium adducts examined in this study have the structure of dimeric monoester complex anti-[Os₂O₄(O₂R)₂] involving Os (VI), as shown in Figure 2.²⁹⁻³¹

Elemental Analysis

The stoichiometry of the reaction of OsO₄ with olefinic C=C double bonds was confirmed by elemental analysis. The results are summarized in Table II. As is evident from the table, the reaction is nearly 100% complete after 24 h. Therefore, the existence of polybutadiene can be investigated by XPS measurement of the Os (VI) involved in sample films prepared under the conditions specified above.

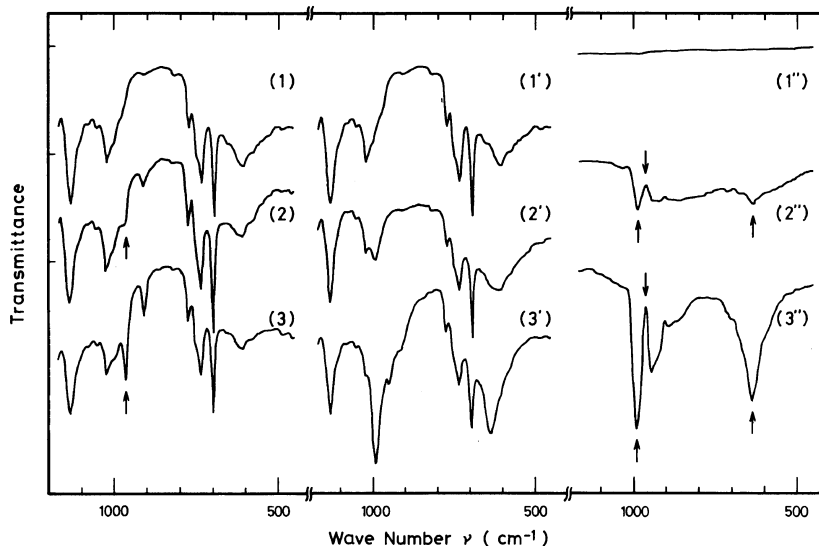


Figure 1. Infrared spectra of (1) PBCL, (2) LBL-4, and (3) LBL-1; (1', 2', 3') after 24 h reaction, (1'', 2'', 3'') difference spectra between spectra before and after reaction.

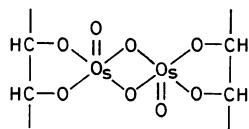


Figure 2. Structure of oxoosmium (VI) dimeric monoester.

Table II. Quantitative data (%) for the addition reaction of osmium tetroxide to olefinic double bonds

Reaction time	LBL-1	LBL-2
40 min	3.8	8.2
1 h	34.1	39.2
24 h	99.0	106.1

XPS Spectra

Figure 3 illustrates a representative Os 4f core level XPS spectra for PBCL and LBL-5 reacted with OsO₄, and for LBL-5 reacted with OsO₄ and then etched for 20 min. The numerical data are tabulated in Table III. The Os 4f spectra have two peaks arising from f-orbital interactions with the electron spin. The indicated curves are all calculated spectra and the best fits to the experimental spectra obtained by applying the non-linear least-squares technique. As is well known,^{12,24,32-35} the binding

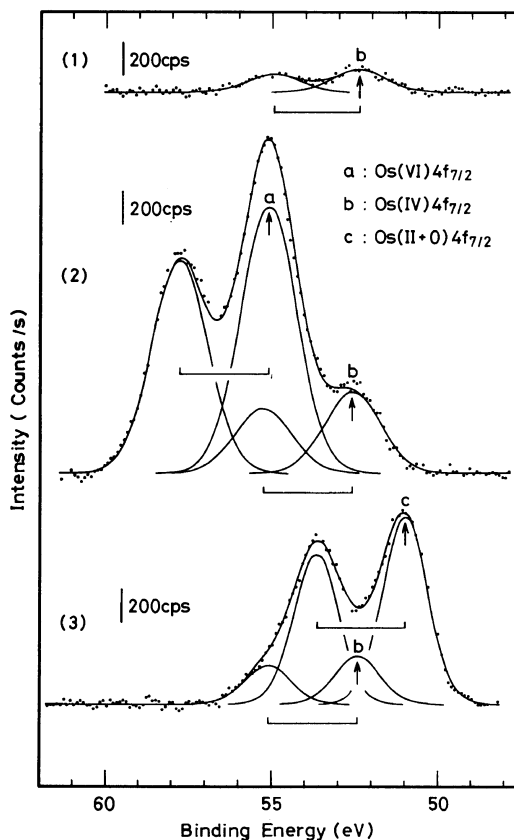


Figure 3. XPS spectra of the OsO₄ addition products of (1) PBCL and (2) LBL-5, and (3) of LBL-5 etched after OsO₄ addition.

Table III. Binding energies for Os4f_{7/2} peaks, peak area ratios, and copolymer compositions calculated from the XPS data

Designation	Binding energies/eV			Area ratio	Butadiene
	(VI)	(IV)	(II+O)	I(Os4f _{7/2})/I(Cl)s	mol%
LBL-5	55.1	52.6	—	0.19	21
LBL-5 (10 min Etching)	—	52.0	50.8	0.13	19
LBL-5 (20 min Etching)	—	52.4	51.0	0.09	12
PBCL	—	52.4	—	0.0	0

energies of Os 4f doublets vary with the oxidation states of Os. In Figure 3, *a*, *b* and *c* represent the 4f_{7/2} peak positions of Os (VI), Os (IV), and Os (II+O), *i.e.*, a mixture of Os (II) and Os (O), respectively. The spectrum for the PBCL homopolymer shows a weak peak for the Os (IV) 4f_{7/2}. On the other hand, the spectrum for LBL-5 has two peaks for Os (IV) 4f_{7/2} and Os (VI) 4f_{7/2}. The existence of the clear peak for Os (VI) 4f_{7/2} demonstrates that the LBL-5 block copolymer membrane has polybutadiene domains at the outermost surface. The *b* peaks for Os (IV) 4f_{7/2}, appearing in both PBCL and LBL-5, seem to be the physical adsorbate of OsO₂ reduced during the addition reaction of OsO₄. By etching, the removal of surface Os and Os reduction probably take place in the polymer surface. As a result, the peak for Os (VI) 4f_{7/2} disappears and shifts to the peaks corresponding to Os (IV) 4f_{7/2} and Os (II+O) 4f_{7/2} core levels.

The ratio of the peak area for Os 4f_{7/2} to that of Cls and surface compositions calculated from the XPS data are summarized in Table III. For the calculation of area ratios for samples before etching, the peak area for Os (IV) 4f_{7/2} was subtracted from the total peak area for Os 4f_{7/2} in order to make correction for the physical adsorbates. After etching, however, the total peak area for Os 4f_{7/2} was used for the calculations. It may reasonably be supposed that Os (VI) 4f_{7/2} was reduced to a mixture of Os (IV) 4f_{7/2} and Os (II+O) 4f_{7/2}, since the physical adsorbates of OsO₂ could be removed by etching.

The PB surface composition of LBL-5 evaluated

Table IV. Binding energies and area ratios for Cls peaks calculated from the XPS data

Designation	Binding energies/eV			Area ratios
	<i>a</i>	<i>b</i>	<i>c</i>	<i>c</i> /(<i>a</i> + <i>b</i> + <i>c</i>) × 10 ²
LBL-5	285.0	286.3	287.7	4.2
LBL-1	285.0	286.4	287.9	4.5
PBCL	285.0	286.4	287.8	3.4

by the area ratio is about twice that of 11.9 mol% in the bulk, but gradually approaches the bulk composition by etching.

The binding energies for Cls peaks and the peak area ratios calculated from the XPS data are shown in Table IV. The Cls core level was divided into three peaks which were the best fits to the experimental spectra obtained in this study. The ratios of the *c* peak area to the total Cls peak area are summarized in the last column of Table IV. The *c* peaks are considered to be due to carbonyl carbons, in consideration of their binding energies.²³ Carbonyl carbons exist in both the main chains and side chains of α -helical A block components. Hence, the peak area ratios of the *c* peak to the total Cls peak of LBL block copolymers are expected to be less than that of PBCL. The peak area ratios *c*/(*a*+*b*+*c*) of both LBL-5 and LBL-1, however, are actually larger than that of PBCL. This means that the surfaces of the LBL block copolymers have more CO residues than does that of PBCL.

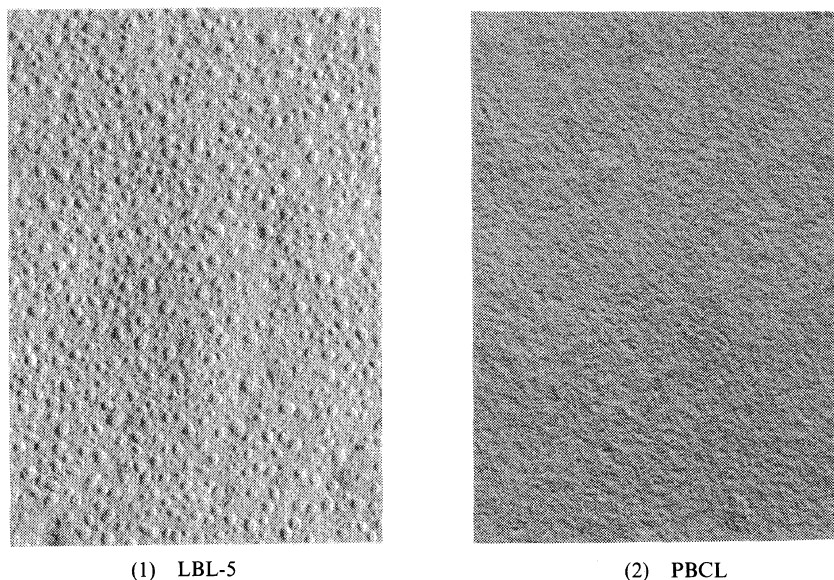
0.5 μm 

Figure 4. Replication electron micrographs for the (1) LBL-5 and (2) PBCL surfaces.

Surface Morphology

Figure 4 shows replication electron micrographs of the membrane surfaces of the LBL-5 block copolymer and PBCL. The shadowing technique was applied to both samples so as to make the contrast more pronounced. The surface of PBCL is almost smooth, whereas that of the LBL-5 block copolymer displays uniform unevenness. From the results of replication electron micrographs made using polystyrene emulsion particles, we confirmed that these circular parts in LBL-5 are convexities raised above a relatively flat matrix phase. We speculate from the sizes of the convex domains and the molar composition of the LBL-5 block copolymer that the convex domains of PB are dispersed on the planar matrix phase of PBCL.

Wettability

In order to obtain more information on the outermost surfaces, measurement was made of the contact angles θ of water for the PBCL and the LBL block copolymer surfaces, as shown in Table V. The contact angles for the LBL block copolymers were found to be smaller than that for PBCL, indicating better wettability. This tendency was noted to be

Table V. Contact angles θ of water for PBCL and LBL block copolymer surfaces at 20°C

Designation	Butadiene	Contact angle
	mol%	degrees
LBL-1	52.3	68.5 ± 0.5
LBL-2	42.3	69.0 ± 0.5
LBL-3	23.7	68.2 ± 0.4
LBL-4	16.2	68.8 ± 0.3
LBL-5	11.9	66.4 ± 0.3
PBCL	0.0	71.4 ± 0.4

especially remarkable for LBL-5.

Figure 5 shows Zisman's plots of $\cos \theta$ versus the surface tension, γ_L , of various liquids for PBCL and the LBL-5 block copolymer. The wettability of LBL-5 is better than that of PBCL; that is, the contact angles for LBL-5 are less. From Figure 5, both PBCL and LBL-5 were found to have critical surface tensions γ_c of 41 dyn cm^{-1} . The γ_c estimated experimentally is a characteristic quantity of a polymer surface. The value of γ_c for poly(*trans*-1,4-butadiene) has been reported to be 31 dyn cm^{-1} by

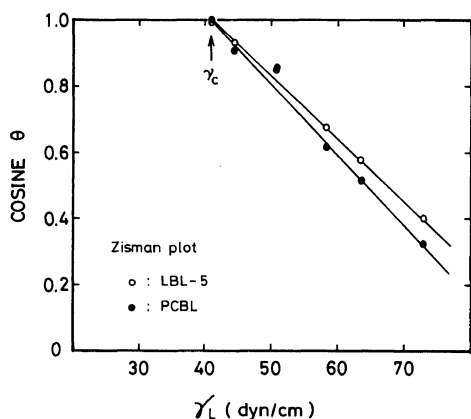


Figure 5. Wettability of LBL-5 and PBCL surfaces with various liquids.

Lee.³⁶ Therefore, it may be concluded that poly(*trans*-1,4-butadiene) (PB) is more hydrophobic than PBCL. The LBL-5 block copolymer is composed of PBCL and PB, and accordingly, the contact angles for LBL-5 should be between those of PBCL and PB. As evident from Figure 5, however, the wettability of LBL-5 is better than that of PBCL. Two factors contributing to this may be proposed: surface roughness, and the existence of many residues capable of forming hydrogen bonds at the LBL-5 surface.

The surface roughness is expressed in terms of Wenzel's "roughness factor," r , which can be evaluated from,³⁷

$$\cos \theta_w = r \cos \theta \quad (4)$$

where θ_w and θ are the apparent and true contact angles, respectively. r is defined as,

$$r = \frac{\Omega}{A} \quad (5)$$

where Ω is the area of an actual surface, and A is the projection of the actual surface on the plane. From the results of replication electron micrographs, we suppose that the surface topography of LBL-5 is something like that shown in Figure 6. The upper and lower sketches of Figure 6 are the plane figure and the cross section figure, respectively. It is assumed that the convexities are parts of the spherical surfaces and are arranged in a hexagonal pattern. The surface area, s , of the convex domain is given by,³⁸

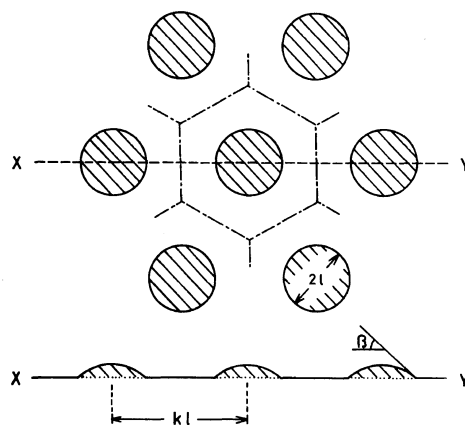


Figure 6. Model for surface topography of LBL-5.

$$S = \frac{2\pi l^2}{1 + \cos \beta} \quad (6)$$

where l is the radius of the projection of the convex domain, and β is the angle between the convex surface and the projection plane. Furthermore, β is given by,

$$\beta = \sin^{-1} \frac{l \sin 2\delta}{2(\sqrt{a^2 + l^2} \cos^2 \delta - a \cos \delta)} \quad (7)$$

where δ is the shadowing angle, and a is the length of the shadow. The derivation of eq 7 is given in the Appendix. In this model, Wenzel's roughness factor is expressed as,

$$r = \frac{A + S - \pi l^2}{A} \quad (8)$$

The projection area, A , is evident from Figure 6, and may be expressed as,

$$A = \frac{\sqrt{3}}{2} k^2 l^2 \quad (9)$$

where k is the experimental constant shown in Figure 6.

Putting eq 6 and 9 into eq 8, and rearranging, we finally obtain the roughness factor for this model as,

$$r = 1 + \frac{2\pi}{\sqrt{3} k^2} \tan^2 \frac{\beta}{2} \quad (10)$$

The observed values in replication electron micrographs for the LBL-5 surface were inserted into eq 10. Thus, we obtain $r=1.063$ for LBL-5. Consequently, from the values of r and the apparent contact angle of water for LBL-5, $\theta_w=66.4^\circ$, we

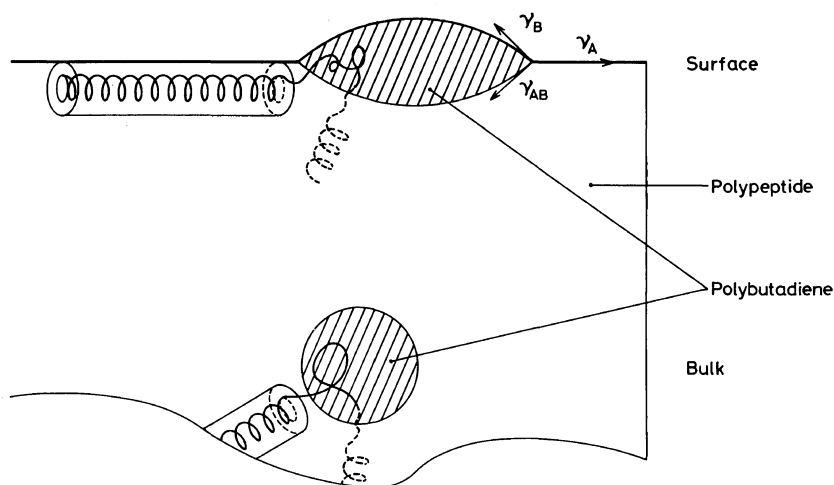


Figure 7. Cross section model for the LBL-5 surface layer.

obtain the true contact angle θ as 67.9° by applying eq 4. We assume $\theta_w = \theta = 71.4^\circ$ for the water-PBCL system, since the PBCL surface is regarded as smooth from the replication electron micrographs. The true contact angle θ , 67.9° , for LBL-5 is still less than 71.4° for PBCL. Thus, the contribution of surface roughness is not sufficient to explain the good wettability of LBL-5.

Hence, the reason for this good wettability should be the fact that the concentration of the residues capable of forming hydrogen bonds (*i.e.*, CO residues) is greater at the LBL-5 surface. This is in accord with the XPS measurement results.

The surface tension of each cast-solvent ($\gamma_{CF} = 27.3 \text{ dyn cm}^{-1}$ at 20°C , $\delta_{TFE} = 20.6 \text{ dyn cm}^{-1}$ at 32.5°C) is less than the critical surface tension of either PB ($\gamma_c = 31 \text{ dyn cm}^{-1}$ at 20°C)³⁶ or PBCL ($\gamma_c = 41 \text{ dyn cm}^{-1}$ at 20°C). These block copolymers are thus considered to be negatively adsorbed onto the solution surface. It seems reasonable to assume that the formation of micelles takes priority over the molecular adsorption on the solution surface of the polymer solution. The shape of these LBL-5 micelles is spherical, *i.e.*, the outer domain of each micelle consists of PBCL block components, as was shown in the preceding paper.¹³ The α -helical PBCL rods should take on greater stability when arranged parallel to the solution surface. These factors may result in the destruction of the micelles. The PB domains have a surface energy lower than the PBCL domains, and thus should appear on the surface.

These features are schematically illustrated in Figure 7. The surface tensions (γ_A , γ_B) of A and B components, and the interfacial tension (γ_{AB}) between A and B components are mutually balanced at the polymer-air interface. Thus, the PB domains may deform like lenses at the polymer surface, as shown in Figure 7. This surface structure certainly contributes to the surface excess of PB components on XPS measurements. Apparently in this model, the interfacial regions between the α -helical A component and the B component appear at the surface. As described above, these regions consist of coiled peptide residues near the end of the polypeptide chain and the terminal residues of amine-terminated polybutadiene. Hence, there are NH and CO residues not incorporated into the intramolecular hydrogen bondings of the α -helix of a polypeptide backbone. Owing to the existence of these regions, the surface of LBL-5 must contain more carbonyl carbons than that of PBCL. The better wettability of water for LBL-5 than for PBCL should support the existence of interfacial regions at the surface.

CONCLUSIONS

XPS, replication electron micrographs, and contact angles were used to investigate the surface morphology of the membranes of PBCL and LBL block copolymers. Our conclusions in regard to LBL-5 are summarized as follows:

1. The microheterophase structure exists on the

surface of LBL-5, whereas the chemical compositions differ considerably from that in the bulk, *i.e.*, the molar fractions of PB are appreciably richer at the surface than in bulk.

2. The PB domains rise above the PBCL matrix in the manner of convex lenses.

3. Interfacial regions between A component and B component are situated at the surface. The surface properties are influenced considerably by these regions.

Similar surface studies are now in progress on other copolymers of different chemical composition and block components.

Acknowledgments. We should like to thank Dr. H. Yamada, the Département of Industrial Chemistry, Kyoto University, for his assistance in carrying out the XPS measurements. We also extend our appreciation to Mr. S. Yamaguchi, Central Research Laboratory, Daikin Kogyo Co., for helping with the replication electron micrographs.

APPENDIX

The Derivation of β

The idealized cross section of the LBL-5 surface is illustrated in Figure 8. The convex surface is assumed to be a part of the spherical surface. In Figure 8, δ is the shadowing angle, β is the angle between the convex surface and the projection plane, a is the length of the shadow, l is the radius of the projected circle, and c is the radius of the sphere described above. The axes of x and y are fixed, as shown in Figure 8. The direction of the x axis is the same as that of the shadowing.

For the straight line m , the following equation

holds,

$$y = \left(x - \frac{a}{\cos \delta} \right) \tan \delta \quad (\text{A1})$$

The equation for the circle is given by,

$$x^2 + (y + c)^2 = c^2 \quad (\text{A2})$$

From eq A1 and A2, it follows that,

$$x^2 + \left\{ \left(x - \frac{a}{\cos \delta} \right) \tan \delta + c \right\}^2 = c^2 \quad (\text{A3})$$

By multiplying both sides of eq A3 by $\cos^2 \delta$ and arranging them, we obtain,

$$x^2 + 2(c \cos \delta - a \tan \delta) \sin \delta x + a \tan \delta (a \tan \delta - 2c \cos \delta) = 0 \quad (\text{A4})$$

Therefore,

$$x_1 + x_2 = -2(c \cos \delta - a \tan \delta) \sin \delta \quad (\text{A5})$$

and,

$$x_1 x_2 = a \tan \delta (a \tan \delta - 2c \cos \delta) \quad (\text{A6})$$

From Figure 8,

$$x_2 - x_1 = 2l \cos \delta \quad (\text{A7})$$

Combining eq A5, A6, and A7, and dividing them by $\cos^2 \delta$ ($\neq 0$),

$$c^2 \sin^2 \delta + 2ca \cos \delta \tan \delta - (a^2 \tan^2 \delta + l^2) = 0 \quad (\text{A8})$$

Now, $c > 0$. Hence, we obtain,

$$c = \frac{2}{\sin 2\delta} \{ \sqrt{a^2 + l^2 \cos^2 \delta} - a \cos \delta \} \quad (\text{A9})$$

Apparently from Figure 8,

$$\beta = \sin^{-1} \frac{l}{c} \quad (\text{A10})$$

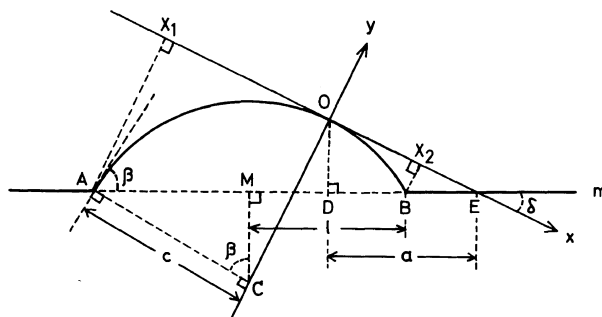


Figure 8. Idealized cross section of the LBL-5 surface.

Substituting eq A9 in eq A10, we finally obtain,

$$\beta = \sin^{-1} \frac{l \sin 2\delta}{2\{\sqrt{a^2 + l^2 \cos^2 \delta} - a \cos \delta\}} \quad (\text{A11})$$

REFERENCES

1. M. Litt and J. Herz, *Polym. Prepr. Am. Chem. Soc., Div. Polym. Chem.*, **10**, 905 (1969).
2. A. K. Rastogi and L. E. St. Pierre, *J. Colloid Interface Sci.*, **31**, 168 (1969).
3. T. C. Kendrick, B. M. Kingston, N. C. Lloyd, and M. J. Owen, *J. Colloid Interface Sci.*, **24**, 135 (1967).
4. E. Vanzo, *J. Polym. Sci., A-1*, **4**, 1727 (1966); *ibid.*, *A-1*, **6**, 1661 (1968); *ibid.*, *C*, **26**, 161 (1969).
5. J. L. Brash and S. Uniyal, *J. Polym. Sci., Polym. Symp.*, No. **66**, 377 (1979).
6. D. T. Clark, J. Peeling and J. J. O'Malley, *J. Polym. Sci., Polym. Chem. Ed.*, **14**, 543 (1976).
7. H. R. Thomas and J. J. O'Malley, *Macromolecules*, **12**, 323 (1979); J. J. O'Malley, M. R. Thomas and G. M. Lee, *ibid.*, **12**, 996 (1979).
8. C. S. Paik Sung, C. B. Hu, E. W. Merrill, and E. W. Salzman, *J. Biomed. Mater. Res.*, **12**, 791 (1978); *ibid.*, **13**, 161 (1979); *J. Colloid Interface Sci.*, **76**, 594 (1980); *ibid.*, **80**, 445 (1981).
9. D. T. Clark and W. J. Feast, *J. Macromol. Sci. Rev. Macromol. Chem.*, **C12** (2), 191 (1975).
10. D. T. Clark, "Structural Studies of Macromolecules by Spectroscopic Methods," K. J. Ivin, Ed., Wiley, London, 1979, Chapter 9; "Advances in Polymer Science," H.-J. Cantow *et al.*, Ed., Springer-Verlag, Berlin, 1977; Polymer Surfaces," D. T. Clark and W. J. Feast, Ed., Wiley, London, 1978, Chapter 16.
11. R. W. Phillips and R. H. Dettre, *J. Colloid Interface Sci.*, **56**, 251 (1976).
12. K. Siegbahn *et al.*, "ESCA, Atomic, Molecular and Solid State Structure Studies by Means of Electron Spectroscopy," Almqvist and Wiksells, Boktryckeri AB, Stockholm, Sweden, 1967.
13. K. Kugo, T. Hayashi, and A. Nakajima, *Polym. J.*, **14**, 391 (1982).
14. B. Gallot *et al.*, *Macromol. Chem.*, **177**, 1889 (1976); **177**, 2569 (1976); **178**, 1595 (1977); **178**, 1641 (1977).
15. T. Hayashi, A. G. Walton, and J. M. Anderson, *Macromolecules*, **10**, 346 (1977).
16. T. Hayashi, J. M. Anderson, and P. A. Hiltner, *Macromolecules*, **10**, 352 (1977).
17. E. Nyilas and R. S. Ward, Presented at the International Conference on Polymer Processing, August 15, 1977.
18. J. L. Brash, B. K. Fritzinger and S. D. Bruck, *J. Biomed. Mater. Res.*, **7**, 313 (1973).
19. R. Criegee, *Justus Liebigs Ann. Chem.*, **522**, 75 (1936); R. Criegee, B. Marchand and H. Wannowius, *ibid.*, **550**, 99 (1942).
20. A. A. Khan, J. C. Riemersma, and H. L. Booij, *J. Histochem. Cytochem.*, **9**, 560 (1961); J. C. Riemersma and H. L. Booij, *ibid.*, **10**, 89 (1962); J. C. Riemersma, *ibid.*, **11**, 436 (1963); *Biochim. Biophys. Acta.*, **152**, 718 (1968).
21. J. S. Hanker, D. K. Romanovicz, and H. A. Padykula, *Histochemistry*, **49**, 263 (1976).
22. W. Stoeckenius and S. C. Mahr, *Lab. Invest.*, **14**, 1196 (1965).
23. D. T. Clark *et al.*, *J. Polym. Sci., Polym. Chem. Ed.*, **16**, 791 (1978); *ibid.*, **16**, 3173 (1978).
24. D. L. White, S. B. Andrews, J. W. Faller and R. J. Barnett, *Biochim. Biophys. Acta*, **436**, 577 (1976).
25. H. Berthou and C. K. Jørgensen, *Anal. Chem.*, **47**, 482 (1975).
26. N. K. Adam and G. Jessop, *J. Chem. Soc.*, **127**, 1863 (1925).
27. S. L. Hsu, W. H. Moore, and S. Krimm, *J. Appl. Phys.*, **46**, 4185 (1975).
28. E. D. Korn, *J. Cell Biol.*, **34**, 627 (1967).
29. R. J. Collin, J. Jones, and W. P. Griffith, *J. Chem. Soc., Dalton Trans.*, 1094 (1974).
30. F. L. Phillips and A. C. Skapski, *J. Chem. Soc. Dalton Trans.*, 2586 (1975).
31. R. J. Collin, W. P. Griffith, F. L. Phillips, and A. C. Skapski, *Biochim. Biophys. Acta*, **320**, 745 (1973).
32. J. Hedman *et al.*, *Phys. Stat. Sol.*, (b) **93**, K103 (1979).
33. G. J. Leigh and W. Bremser, *J. Chem. Soc. Dalton Trans.*, 1216 (1972).
34. C. K. Jørgensen, *Theoret. Chim. Acta*, **24**, 241 (1972).
35. P. Burroughs, S. Evans, A. Hamnett, A. F. Orchard, and W. V. Richardson, *J. Chem. Soc. Faraday Trans. 2*, **70**, 1895 (1974).
36. L.-H. Lee, *J. Polym. Sci., A-2*, **5**, 1103 (1967).
37. R. N. Wenzel, *Ind. Eng. Chem.*, **28**, 988 (1936).
38. W. A. Zisman, "Contact Angle, Wettability and Adhesion," Advances in Chemistry Series, No. 43, 1964, p 115.